International Journal of Microwave and Wireless Technologies

cambridge.org/mrf

Multiband antenna design based on Gosper fractal for implantable biomedical devices

Rajeev Kumar, Surinder Singh and Ajay pal Singh Chauhan

Department of Electronics and Communication Engineering, Sant Longowal Institute of Engineering and Technology, Longowal, Sangrur 148106, Punjab, India

Research Paper

Cite this article: Kumar R, Singh S, Singh Chauhan A (2022). Multiband antenna design based on Gosper fractal for implantable biomedical devices. *International Journal of Microwave and Wireless Technologies* **14**, 970–980. https://doi.org/10.1017/S1759078721001203

Received: 14 March 2021
Revised: 21 July 2021
Accepted: 23 July 2021
First published online: 16 August 2021

Key words:
Biomedical telemetry; Gosper curve fractal; human tissue model; link budget; multiband antenna

Author for correspondence:
Surinder Singh,
E-mail: surinder_sodhi@rediffmail.com

Abstract

In this paper, a novel multiband implantable planar inverted-F antenna (PIFA) antenna based on Gosper curve fractal geometry is designed for biomedical telemetry applications. The antenna has covered four dedicated frequency bands; medical implant communication system band (MICS 402–405 MHz), industrial, scientific, and medical bands (ISM 902–928 MHz and 2.4–2.5 GHz), and wireless medical telemetry services (WMTS 1395–1400 and 1429–1432 MHz). The proposed antenna is designed on Rogers RO 3010 substrate of thickness 25 mil and volume equal to 153.67 mm^3. The reflection coefficient and the radiation pattern are measured inside muscle-mimicking liquid tissue phantom. The antenna has achieved the impedance bandwidth of 126, 406, 168, and 175 MHz at MICS (403 MHz), ISM (915 MHz), WMTS (1400 MHz), and ISM (2.45 GHz) with maximum gain value −33.6, −21.04, −15.48, and −10.25 dBi, respectively. The data link range between the implantable antenna and off body antenna has been performed with −16 dBm input power. Additionally, the obtained specific absorption rate with the input of 25 μW power has also been obtained within the safety limit and hence ensures the reliability of the proposed antenna.

Introduction

Wireless body area network (WBAN) devices for biomedical telemetry applications are developing rapidly, making it possible to monitor human beings' health without admitting them to the hospital. An implantable medical device serves as WBAN nodes and communicates with an external device by sensing vital physiological changes and symptoms inside the human body. A robust but flexible and miniature size antenna can establish a reliable wireless link between various WBAN nodes. The designing of an implantable antenna, which must perform inside the human body, is more challenging than an antenna in free space. The first challenge is to make the antenna miniature in size. Secondly, a wide impedance bandwidth is required as the antenna is surrounded by frequency-dependent tissues (high permittivity medium) and can experience wide permittivity diversity for different body tissue environments or even permittivity of tissue can vary from person to person. However, antennas with small bandwidth have also been proposed in [1, 2], which can be reliable for only a single tissue environment. Thirdly, as the human tissue has a high absorption capability ($\sigma \neq 0$) of electromagnetic waves, an antenna must communicate well inside the human tissue environment in prescribed safety specific absorption rate (SAR) limit. To avoid internal tissue damage or infection, proper isolation of an antenna using biocompatible material should also be taken into design consideration. Finally, the antenna should be designed for the allotted frequency band for medical implants in consideration of body tissues.

The frequency allocations for WBAN devices for biomedical telemetry applications are controlled by various organizations worldwide [3]. Federal communication commission (FCC) recommends medical implant communication system (MICS) band (402–405 MHz), Med radio band (401–406 MHz) with an extension of 1 MHz on both sides of the MICS band, and 24 MHz of extended-spectrum in between 413 and 457 MHz on a secondary basis. Both implantable medical devices and body-worn devices use Med radio spectrum band for diagnostic and therapeutic purposes. Another medical telemetry service run by FCC is wireless medical telemetry service (WMTS). The spectrum used for the WMTS band contains 14 MHz of the spectrum from 608–614, 1395–1400, and 1429–1432 MHz [4]. These bands are used for TV channels for indoor communication and remote monitoring of patients far from the hospital. International telecommunication union radiocommunication (ITU-R) has provided a spectrum for industrial, scientific, and medical (ISM) applications [5]. ISM band from 433.1–434.8, 868–868.6, 902–928, and 2.4–2.5 GHz is also recommended for the biomedical telemetry of medical implants.

The reported implantable antennas are focused on size reduction for only single or dual-band operation in the last decade, although there is still hope in further size reduction [6–12]. A dual-band antenna using serpentine line planar inverted-F antenna (PIFA) design for glucose level testing is reported in [6] with achieved resonance bandwidth of 35 and 7.1% at MICS and ISM bands, respectively, with 1265.6 mm^3 volumetric size. They have

CAMBRIDGE UNIVERSITY PRESS

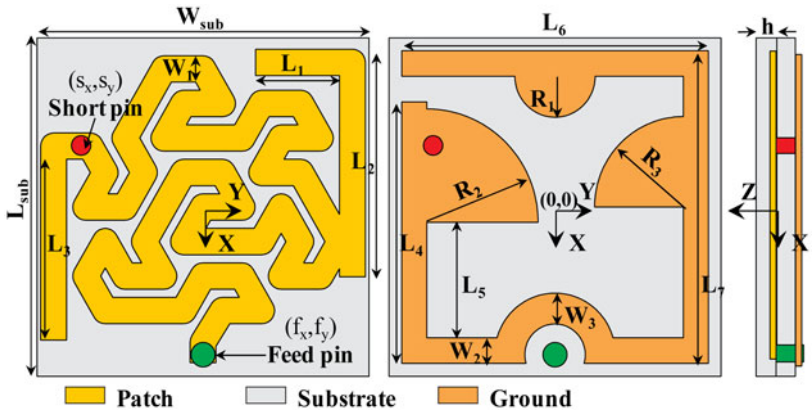

Fig. 1. Structure of the proposed Gosper antenna design.

achieved adequate bandwidth by the use of a thick substrate and a superstrate layer. A spiral-shaped PIFA for the MICS band has been proposed within the volume 2681 mm^3 [8] and 650 mm^3 [9], respectively. Here, the size reduction is achieved by using high permittivity Macor ($\epsilon_r = 6.1$) and Roger RT/duroid 6010 ($\epsilon_r = 10.2$, $\delta = 0.0023$) substrate, respectively. The miniaturization can also be achieved by multilayering of patches combined with PIFA, as reported in [10–12]. The multilayer patch configuration consists of two layers of radiating patch stacked with the ground layer. Both patches are fed with a single feed pin; on the other hand, PIFA configuration is formed by inserting a shorting pin between the lower patch and the ground layer. Further, the lengthening in the current path is achieved by inserting the hooked slot [10], meander path [11] on a circular patch, while [12] uses an Archimedean spiral patch with the volumetric size of 179, 215, and 60 mm^3, respectively. In [13], the antenna is designed on lower dielectric Taconic RF-35 ($\epsilon_r = 3.5$) substrate for improved radiation efficiency, claimed with a volume size of 39.3 mm^3 but for the single band only. The size reduction may lead to a reduction in maximum antenna gain, as reported in [14], having a volumetric size of 31.5 mm^3 for the MICS band and ISM (2.4–2.5 GHz) band with peak gain −39.1 and −21.2 dBi, respectively. However, in the last few years, researchers' attention has been in designing dual/triple-band antennas in parallel, emphasizing size reduction and moderate gain [15–21]. Multiband antennas can support to switch into sleep and wake mode and hence, can reduce the power consumption. On the other side, data transmission and demand can also be controlled by switching between the low data rate at the MICS band and the high data rate at the ISM band. WMTS band is used for remote monitoring of patients far from the hospital. Antenna with the smallest volumetric size is expected so far for implantable application as reported in [16], with 9.8 mm^3 of volume. This dual-band antenna only supports the ISM band 915 MHz and 2.45 GHz but lacks the MICS band. Zada and Yoo [20] support three resonance bands with a volumetric size of 21, but the lowest frequency is 915 MHz. Ref [15] has also presented the tri band antenna for skin implant with a volume of 52.5 mm^3, but suffers from lower gain and bandwidth. It is observed that the area of reported antennas is comparable, but the overall volume can be reduced by considering a thin substrate; on the contrary, a thicker substrate improves the bandwidth.

In this work, we propose a multiband implantable antenna with wideband resonance for biomedical telemetry application. The proposed PIFA antenna is inspired by Gosper curve fractal geometry along with defects in the ground plane. Also, human tissue modeling for numerical investigation and optimization of the proposed antenna model has been carried out. The organization of the paper is as follows. Section "Model and technique" represents the design model and techniques. Final design and analysis is described in section "Final design and analysis". Section "Results and discussion" follows the results and discussion and concluded in section "Conclusion".

Model and technique

Antenna geometry

The proposed quad-band PIFA antenna is shown in Fig. 1. The radiating element of an antenna consists of Gosper curve fractal geometry of width (W_1), which has been mounted on Roger RO 3010 ($\epsilon_r = 10.2$ and $\tan\delta = 0.0035$) substrate of dimension $L_{sub} \times W_{sub}$ and thickness $h = 25$ mil. The overall volume of the final prototype design is approximately equal to 154 mm^3. An inverted L-shaped stub is combined with the Gosper curve that helps in impedance matching and to acquire the essential WMTS band. The additional length L_3 and defected ground plane have also improved the radiation performance of the antenna design with wideband impedance matching performance. The ground plane with defect, form a splitted square ring which is combined with one semi-circle of radius R_1 which is located at $(-L_7/2 + W_2,\ 0)$ and two quarter circles of radius R_2 and R_3, whose centers are located at $(L_7/2 - (W_2 + L_5),\ -L_6/2 + W_2))$ and $(0,\ L_6/2 - W_2))$, respectively. The split gap is a square with a value with a dimension of each side equal to W_2. The PIFA antenna is formed by connecting the radiating patch with the ground plane at (S_x, S_y). The antenna is fed with 50 Ω coaxial probe located at (f_x, f_y). To avoid physical contact between human tissues with the radiating element, a superstrate layer of the same dimension as a substrate layer is used. The dimension detail of all the parameters of the proposed antenna design is tabulated in Table 2.

Antenna design methodology

The conventional size of the radiating element must be equal to half of the resonance wavelength. For the MICS (403 MHz) band, the lowest frequency among all the desired frequency band, the length of antenna radiating element is calculated to be approximately 373 mm in free space and 50–55 mm in human muscle ($\epsilon_r = 57.1$) or skin tissue ($\epsilon_r = 46.7$) [22, 23]. Further, the antenna length is inversely proportional to the square root of the permittivity of the antenna substrate. Hence, the use

https://doi.org/10.1017/S1759078721001203 Published online by Cambridge University Press

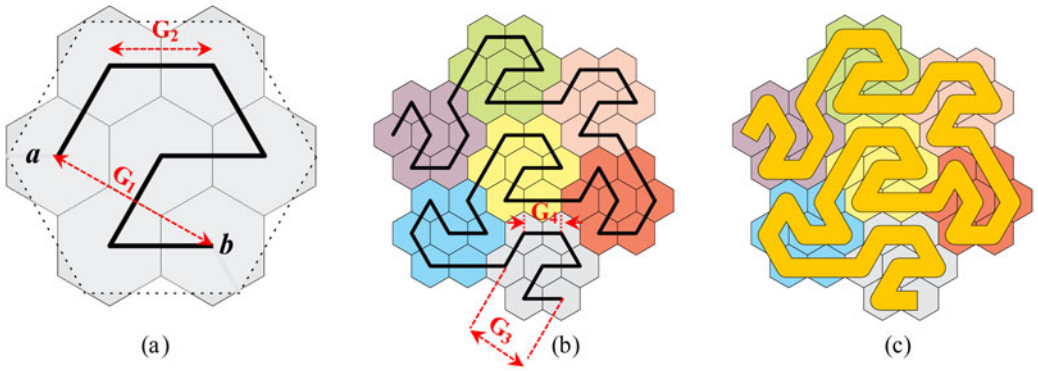

Fig. 2. Gosper curve fractal design geometry, (a) 1st Gosper iteration, (b) 2nd Gosper iteration, (c) model geometry of proposed antenna element.

of a high value of substrate permittivity further promotes the size reduction. We introduce Gosper curve fractal geometry for lengthening of the effective current path on high permittivity substrate. A fractal structure exhibits self-similarity characteristics as well as manifests remarkable space-filling properties. A Gosper curve fractal consists of a flow snake path, constructed by replacing the line segment with self-similar geometry based on a defined algorithm which never intersects even at an infinite limit [24]. The design flow of the antenna element using Gosper curve fractal geometry is illustrated in Fig. 2. Every unit cell, called as node, contains seven hexagons. The unit element of Gosper fractal is obtained by intersecting each hexagon cell's center point in a specific path, as shown in Fig. 2(a). Let's say path A: if proceeds from left to right (*a to b*) and path B: if we move from right to left (*b to a*) crossing through each hexagonal cell. The size of every Gosper fractal geometry is scaled down by $\sqrt{7}$ compared to the previous size, as $G_3 = G_1/\sqrt{7}$ and $G_4 = G_2/\sqrt{7}$. G_1 and G_2's value for the proposed antenna design is taken to be 5.16 and 3.44 mm, respectively. The hexagon of Fig. 2(a) has an edge dimension of 1.72 mm. Here, L-system (Lindenmayer system) tool has been utilized to obtain the Gosper fractal geometry [25].

The L-system assists in representing the self-similar fractal geometries replacing each line segment by a seven-segment generator curve among the seven hexagons group in a recursive manner. However, the dimension and position of each node can be determined based upon previous path A or B. The rule to generate the proposed Gosper fractal design geometry can be described as follows:

For A:$f-r-f-r-f-rr-f-l-f-ll-f$ and

For B:$f-rr-f-r-f-ll-f-l-f-l-f$,

where f inspires to move the unit step in a forward direction, r and l stand for right and left rotation with 60 degrees. The A and B paths blended to form the proposed Gosper fractal and can be represented as shown below.

$$B \leftarrow B-r-f-A-r-f-A-f-l-B-f-l-B-f-B-f-A.$$

Here each segment is scaled down by $\sqrt{7}$ of the previous dimension. However, the initial coordinate must have to define before the curve generation. The proposed design contains a meandering path that fills the two-dimensional space without touching any infinite limit that helps to lengthen the radiating element's electrical length. Finally, the proposed path is swiped with appropriate thickness, as illustrated in Fig. 2(c).

Table 1. Parametric constant values of proposed human tissue model for determination of permittivity and conductivity in the frequency range 200 MHz to 3 GHz

	Permittivity		Conductivity	
Human tissue	*p*	*q*	*p*	*q*
Muscle	2.61×10^{-4}	8.67×10^{-4}	11.27	−0.495
Skin	-3.47×10^{-2}	2.83×10^{-3}	11.34	−0.493
Fat	7.64×10^{-3}	3.93×10^{-3}	99.5	−4.42
Bone	-6.37×10^{-2}	5.44×10^{-3}	31.07	−1.38

Numerical tissue model

To investigate the implantable antenna's performance, a numerical tissue model that mimics to real human tissue in an electromagnetic (EM) medium is required. The EM properties, such as permittivity, conductivity, attenuation constant, loss tangent, etc., of human tissues are frequency-dependent, so proper modeling is desirable for antenna characterization. The simplest way to define the numerical tissue model is a homogeneous anatomical model assigned with electrical parameters at its center frequency of band of interest. As in [26], the permittivity and conductivity of human skin tissue at 402 MHz and 2.44 GHz are taken as (ϵ_r = 46.7, σ = 0.69 S/m) and (ϵ_r = 38.04, σ = 1.44 S/m), respectively. The muscle tissue properties at 402 MHz (ϵ_r = 57.11, σ = 0.79 S/m) and 433 MHz (ϵ_r = 56.84, σ = 0.804 S/m) are considered in [12], for numerical investigation of spiral antenna. These values are commonly adopted from the inclusive and most preferred database source of human body properties presented by Gabriel *et al.* [27, 28].

Specially, single-point parameters may lead to incorrect results and interfere with a multiband antenna design. Therefore, for proper characterization, the tissue model must express the correct dielectric values at its respective frequency. As in [29], three-pole cole-cole model equation has been proposed to manifest the human skin tissue modeling, but it requires strenuous effort due to complicated function. Therefore, a simple frequency-dependent model for human tissue permittivity and conductivity to characterize the proposed quad-band antenna is proposed. Here, human muscle, skin, fat, and bone tissues are expressed as a function of frequency by taking the database of Gabriel *et al.* [27, 28] as a reference. The permittivity and the conductivity of human tissue can be represented by a very simplified reciprocal

https://doi.org/10.1017/S1759078721001203 Published online by Cambridge University Press

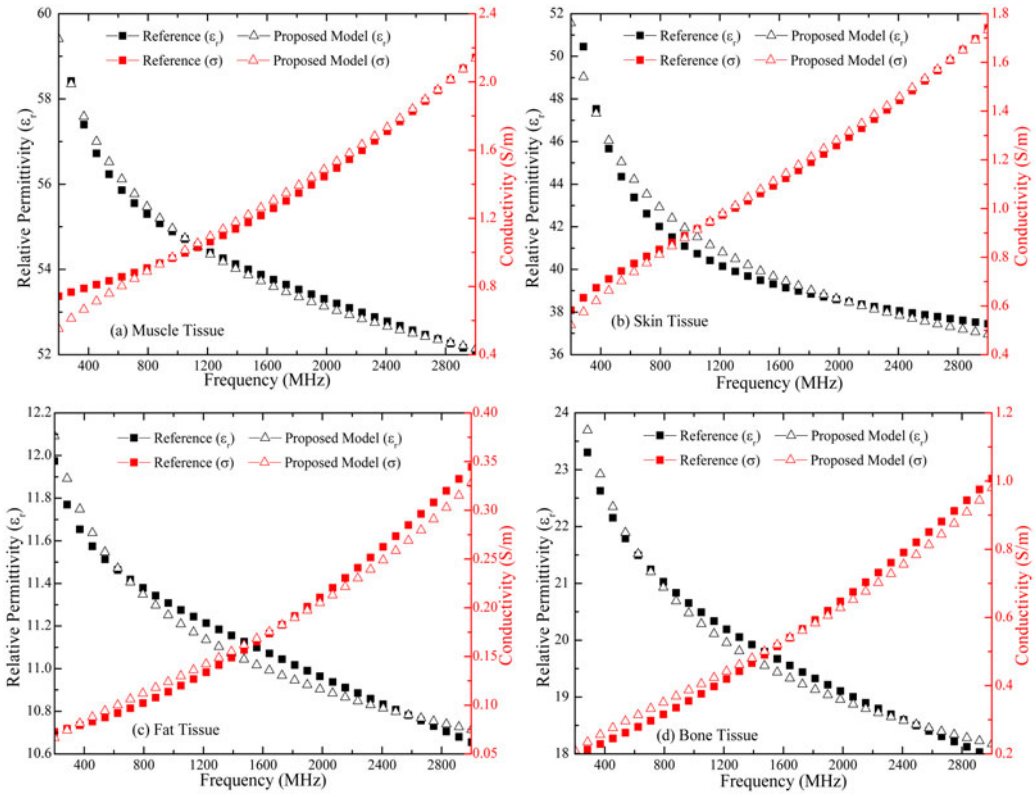

Fig. 3. Comparison of relative permittivity and conductivity of proposed human tissue model with the reference value taken from [27, 28], (a) muscle tissue, (b) skin tissue, (c) fat tissue, and (d) Bone tissue.

logarithmic equation, which can be expressed as:

$$Y(f_r) = \frac{1}{p + q\ln(f_r)}, \quad (1)$$

where $Y(f_r)$ is the permittivity or conductivity of human tissue at a frequency (f_r). p and q are the constants representing the respective tissue property in the frequency range 200 MHz to 3 GHz. The values of these constants are expressed in Table 1 and the proposed models fitted with Gabriel *et al.* are illustrated in Fig. 3. The antenna is initially placed inside a single-layer muscle tissue model and is finally optimized inside the multilayer cylindrical human arm model [21].

Final design and analysis

Antenna design optimization

We proceed with the initial antenna design modeled inside a homogeneous muscle tissue model with a fixed value of permittivity and conductivity at the MICS band, then optimized inside the multilayer frequency-dependent arm tissue model. The antenna design consists of 20 variables, out of which 14 have been utilized for optimization. Sequential nonlinear optimization model is utilized with 101 numbers of iterations. The cost function interprets the reflection coefficient (S_{11}) of antenna design to achieve the goal of −20 dB with weight (1) for all four desired frequency bands centered at 403, 915, 1400, and 2450 MHz. The range of all variables under the optimization constraints and the final optimized dimension are outlined in Table 2. For the ease of simplicity, the aspect ratio of length and the width of both substrate and the ground are kept constant.

Parametric analysis

To express the behavior of dimensions on antenna performance, a parametric investigation has been utilized. Figures 4 and 5 show the effect of width W_1 and W_2, respectively. While increasing W_1, an increment in the resonance frequency of the 3rd and 4th bands has been observed. On the other side, W_2 can only tune the third frequency band but helps in the impedance matching.

The circle embedded with the ground plan also plays a significant role in impedance matching. The effect of radius R_1, R_2, and R_3 between 0 and 4 mm on the resonance frequency of four desired medical bands is illustrated in Fig. 6. The vertical axis's left section shows the minimum value of S_{11}, which is considered below −10 dB; while the right side shows the resonance frequency at S_{11} (min) point. The result shows minimal shifting in resonating frequency in every band until R_1 reaches 2.5 mm. When the radius increases after 2.5 mm, it gets connected with either circle 2 or 3, resulting in frequency decrement. The quarter circle shape of circles 2 and 3 is taken to increase the electrical length of the ground plane. An increment in R_1 helps to decrease the resonance frequency for the first and second bands without affecting the other higher band. On the other side, R_2 helps to increase the resonance frequency at the second band, but at the same time, other bands somewhat decrease slightly. R_3 improves the matching, especially for third and fourth bands without affecting the bandwidth

https://doi.org/10.1017/S1759078721001203 Published online by Cambridge University Press

Table 2. Parametric detail of proposed Gosper antenna design with initial and optimized value in (mm)

Symbol	Initial value	Optimization range	Optimized value for fabrication	Symbol	Initial value	Optimization range	Optimized value for fabrication
L_{sub}	12	10–12	11	W_1	1	0.6–1	0.85
W_{sub}	12	10–12	11	W_2	1	0.5–1.5	0.83
H	25 mil	–	25 mil	W_3	1	–	1
L_1	0	0–5	3.64	R_1	2.5	1–4	1.33
L_2	7.4	–	7.4	R_2	2.5	1–4	3.69
L_3	5	5–7	6.73	R_3	2.5	1–4	2.94
L_4	8	–	8.5	f_x	4.5	4.5–5	−4.8
L_5	3	–	3.75	f_y	0	–	0
L_6	10	10–11	10.16	S_x	−2	–	−2
L_7	10	10–11	10.16	S_y	−4.5	−4.5 to −3.5	−4.04

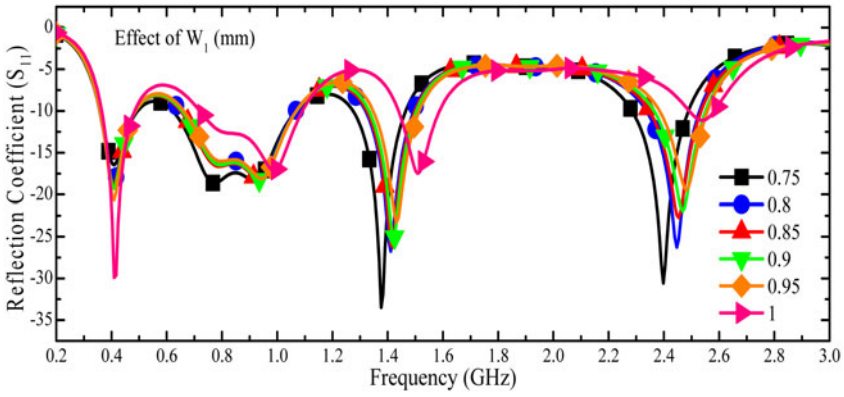

Fig. 4. Effect of Gosper curve width (W_1) on resonance frequency of proposed Gosper antenna design.

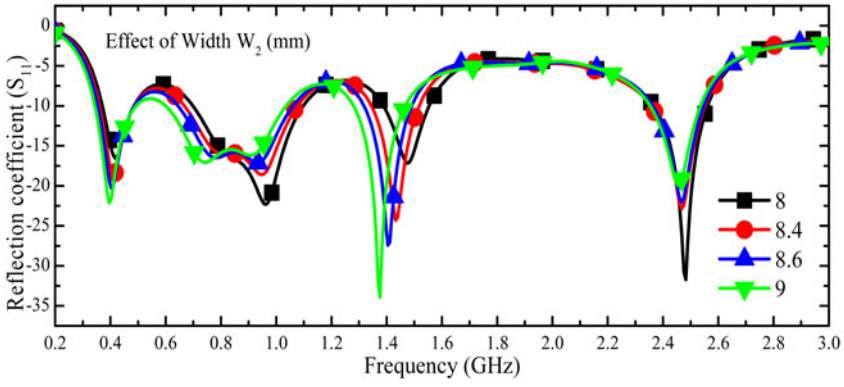

Fig. 5. Effect of ground width (W_2) on resonance frequency of proposed Gosper antenna design.

and the resonance frequency. The final optimized dimension of R_1, R_2, and R_3 is taken to be 1.33, 3.69, and 2.94 mm, respectively.

Figure 7 shows the reflection coefficient response of six different parametric conditions of the antenna design model. The graph response also depicts the stepwise design modification model of the proposed antenna design. Implementation of a defect in the ground plan significantly helps to achieve the entire desired frequency band. Additional arm length L_1 improves the radiation characteristics while L_2 and L_3 support to achieve the WMTS band centered at 1400 MHz. However, without any other arms, Gosper gives the first resonance bandwidth of approximately 600 MHz along with ISM (2.45 GHz) band.

Effect of permittivity of tissue

The permittivity of human tissue is different for different organs and it depends upon the quantity of water contains. The human body contains verity of complex constituents of tissues, having large variation in permittivity range. Therefore, in this section, the proposed antenna model's resonance characteristic has been analyzed inside lossy tissue medium mimic to human tissues with a permittivity (ϵ_r) range from 20 to 70. Figure 8 shows the effect of resonance frequency on all proposed resonant frequency bands and on its bandwidth. As anticipated, the resonant frequency of all bands decreased with the permittivity, but larger

https://doi.org/10.1017/S1759078721001203 Published online by Cambridge University Press

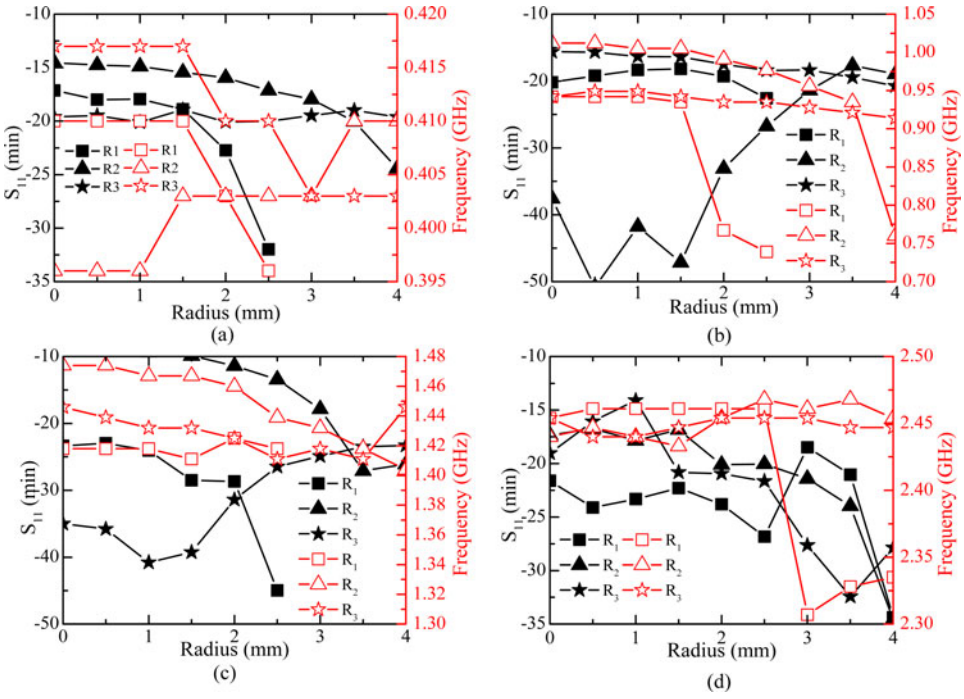

Fig. 6. Parametric effect of radius (R_1, R_2, R_3) of circles present in ground plane at various frequency bands; (a) MICS band, (b) ISM (915 MHz) band, (c) WMTS band (1.4 GHz, (d) ISM (2.45 GHz).

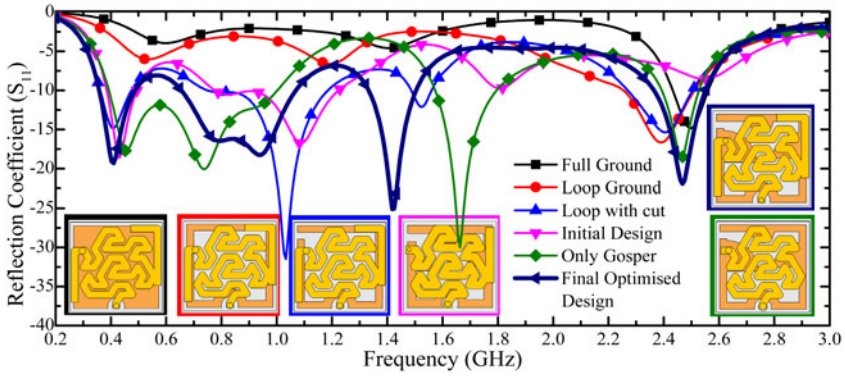

Fig. 7. Comparison of reflection coefficient response of various configurations of Gosper antenna during antenna design modeling.

frequency shifting has been found in the third resonant band than the other three. The fluctuation has been found at the second band due to the establishment of dual resonance characteristics and hence the obtained bandwidth is also large compared to others. It is also essential to see that the frequency shifting is lesser than the achieved bandwidth even if the frequency is shifting. Finally, the result shows that the proposed antenna can be used successfully inside the tissue having permittivity (ϵ_r) from 20 to 70 with some limitation on the third resonance band.

Results and discussion

Figures 9(a)–9(d) show the fabricated prototype of the proposed Gosper antenna design. The antenna is fabricated on Rogers RO 3010 substrate using a chemical etching process and fed via 50 Ω RG 86 semi-rigid coaxial cable with SMA F connector. The superstrate layer is fixed on top of the radiating element with Araldite adhesive. Further, the antenna is implanted inside a muscle tissue-mimicking liquid phantom to analyze the antenna performance. The phantom comprises deionized water, sugar, and salt (1 g per 200 ml solution) [6]. Figures 9(e) and 9(f) show the experimental setup to measure the reflection coefficient and radiation pattern. PNA L N5232B Network analyzer is used for antenna testing and measurement.

Reflection coefficient

Figure 10 shows the reflection coefficient response of the proposed multiband Gosper antenna. As a result, the antenna performance inside both reference tissue and the proposed tissue model is very analogous. Furthermore, the measured reflection coefficient inside muscle-mimicking liquid phantom also expresses a competent result. The proposed antenna design is compared with the previously reported kinds of literature in terms of size, frequency band, bandwidth, gain, etc., tabulated in Table 4. Comparative to the entire, the proposed antenna is able to achieve four dedicated frequency bands with the bandwidth of 126, 406, 168, and 175 MHz which provides sufficient bandwidth to serve in variant dielectric environments.

Radiation characteristics

The radiation performance of the proposed antenna is analyzed inside the proposed tissue model. Figure 11 shows the 2D (a–d)

https://doi.org/10.1017/S1759078721001203 Published online by Cambridge University Press

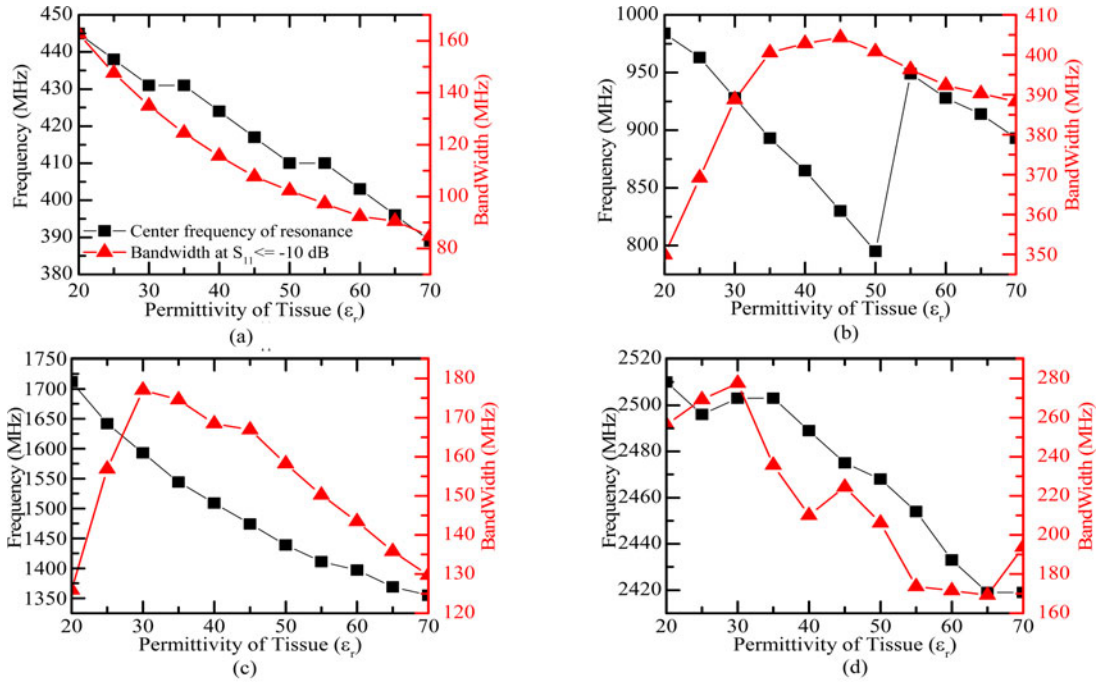

Fig. 8. Effect of effective permittivity of tissue phantom on antenna resonance frequency and bandwidth; (a) MICS (403 MHz) band, (b) ISM (915 MHz) band, (c) WMTS (1400 MHz) band, (d) ISM (2.45 GHz) band.

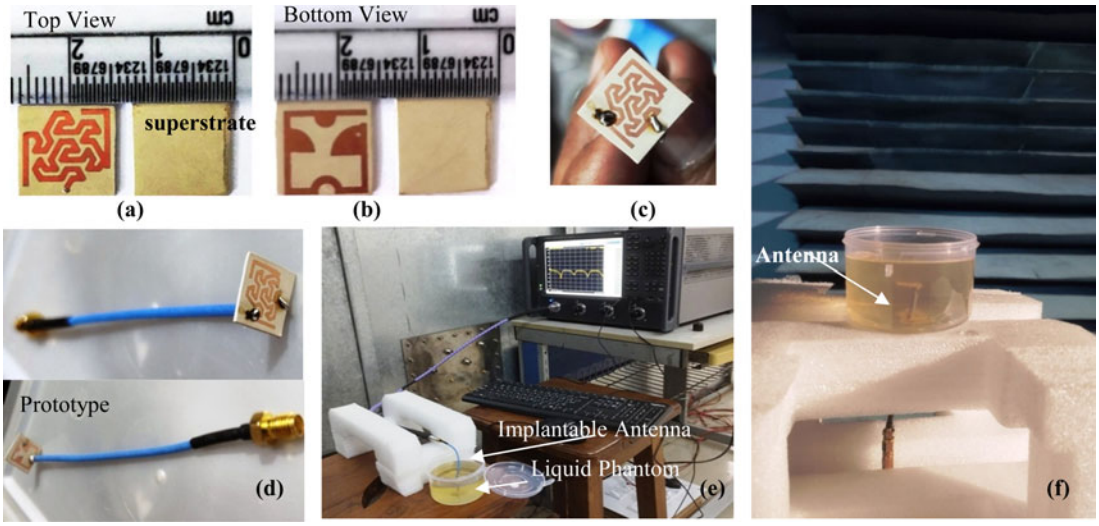

Fig. 9. (a–d) Fabricated prototype of proposed antenna, measurement setup for (e) reflection coefficient, and (f) radiation pattern observation.

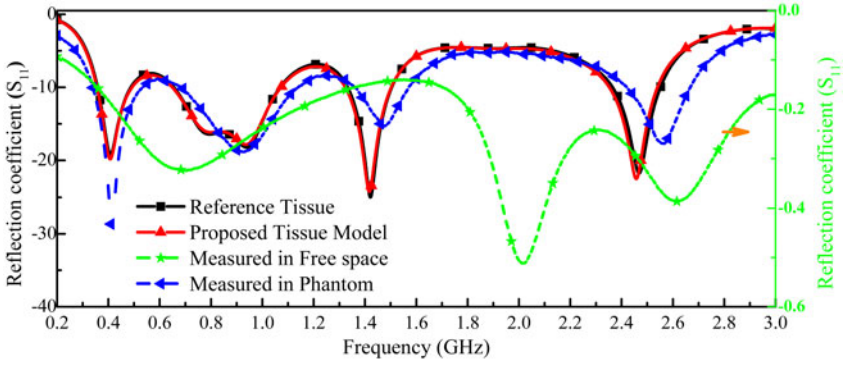

Fig. 10. Reflection coefficient of proposed antenna design.

https://doi.org/10.1017/S1759078721001203 Published online by Cambridge University Press

Table 3. Parameters for link budget calculation

Symbol	Parameters	Unit	Values
f	Operating frequency	MHz	403/915/1400/2450
P_t	Transmitter power	dBm	−16
G_t	Transmitter antenna gain	dBi	−33.6/−21.04/−15.48/−10.25
L_{tx}	Transmission loss	dB	4
L_{path}	Free space path loss	dB	Distance dependent
d	Distance	M	1–15
G_r	Receiver antenna gain	dBi	2.15
k	Boltzmann's constant	Joules/K	1.38×10^{-23}
T	Temperature	Kelvin	293
B	Bandwidth	KHz	300
N_0	Noise power density	dBm/Hz	−173.9
E_b/N_0	Signal to noise per bit (ideal BPSK)	dB	9.6
B_r	Bit rate	kbps	7/1000
	Bit error rate	1/s	1×10^{-5}
LM	Link margin	dB	P_r–P_{req}

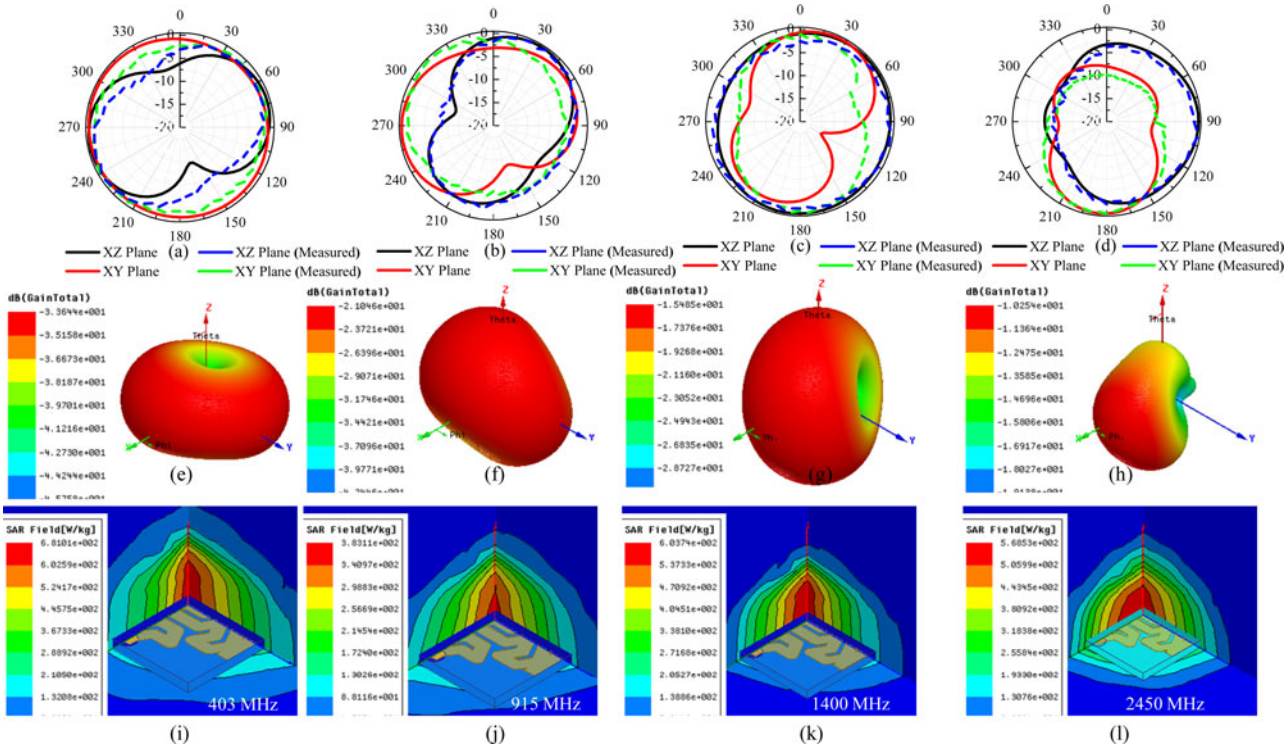

Fig. 11. Radiation characteristics of proposed antenna design at 403, 915, 1400, and 2450 MHz; 2D radiation pattern (a–d), 3D radiation pattern (e–h), specific absorption rate (SAR) (i–l).

and 3D (e–h) far-field gain radiation plot of the proposed Gosper antenna design at 403, 915, 1400, and 2450 MHz, respectively. The radiation pattern of the antenna depends on the tissue's electrical characteristics and its shape and size. Even the position and orientation of implantation also alter the radiation pattern performance. Due to the lossy medium ($\sigma \neq 0$) of the human body and miniature-sized antenna, meager antenna gain has been observed. Maximum gain at 403, 915, 1400, and 2450 MHz are −33.64, −21.04, −15.48, and −10.25 dBi, respectively. Further, regarding the safety of humans due to radio exposure, a power limit has been set for each body centric and implantable wireless device. There are two safety standards for SAR that help to calculate the power absorbed by any lossy medium ($\sigma \neq 0$) in terms of the mass of tissue [30]. In total, 1.6 W/kg is a maximum allowed SAR

https://doi.org/10.1017/S1759078721001203 Published online by Cambridge University Press

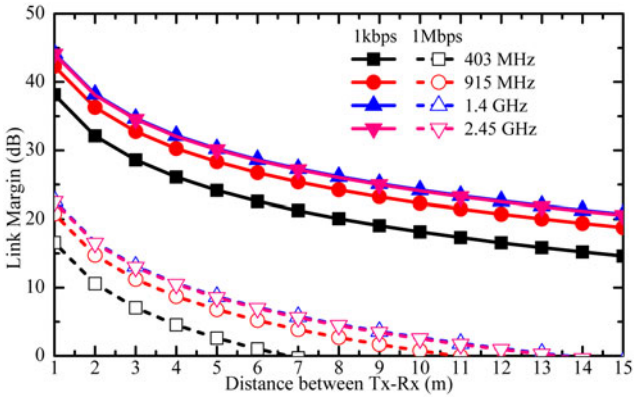

Fig. 12. Link margin of proposed Gosper antenna at different frequencies.

value as per IEEE C95.1-2005 standard, and it is calculated over 1 g of cubic-shaped human tissue [31]. Another SAR standard is adopted by the International Commission on Non-Ionizing Radiation Protection (ICNIRP) over 10 g of human tissue to <2 W/kg. For the proposed antenna when fed with 1 Watt power, the SAR values computed at 403, 915, 1400, and 2450 MHz are 681, 383, 603, and 568 W/kg, respectively, as shown in Figs 11(i)–11(l). To satisfy 1.6 W/kg limit, the allowed power to the antenna must be limited to 2.35 mW. However, the RF power of implantable devices is limited to 25 µW, which is too smaller than the allowed transmitted power. This shows that the proposed antenna design satisfies the SAR regulation limit.

Link budget analysis

The RF signal attribute varies during the transmission of a signal from transmitter to receiver, depending upon factors such as environment, noise, distance, etc. Therefore, a link budget analysis has been carried out between the proposed antenna and the external off-body telemetry system to estimate reliable wireless communication links. Dipole antenna with a realized gain of 2.15 dBi has been taken as base station antenna. The calculated link margin is shown in Fig. 12. Link margin is a benchmark that defines reliable communication's conformation and can be determined by the following expressions [32].

$$P_r = P_t + G_t - L_{tx} - L_{path} + G_r, \tag{2}$$

where P_r (dBm) is the power available at the receiving antenna, P_t (dBm) and G_t (dBi) are transmitted power and gain of the transmitter antenna. The computed radiated power of the proposed antenna at 403 MHz is 1.61 mW when 1 W power is applied, but for safety consideration, the maximum permitted power for an implantable antenna is limited to 25 µW. Therefore, $P_t = 25$ µW (−16 dBm) is taken for further analysis [18]. G_r (dBi) is the gain of receiving antenna, L_{tx} (dB) is the transmitter loss due to connector or cable.

Table 4. Comparison of proposed antenna design with earlier reported antennas.

Ref No.	Frequency	Bandwidth (MHz)	Volume (mm^3)	SAR 1 g avg Max (W/kg)	Max gain (dBi)
[33]	ISM 915 MHz	N/A	14.13	N/A	−25
[15]	MICS 402 MHz	64	52.5	665.3	−40.85
	ISM 915 MHz	91		837.7	−32.98
	ISM 2.45 GHz	105		759.7	−22.37
[17]	MedRadio 402 MHz	165	114.14	666	−41
	ISM 2.45 GHz	680		676	−21.3
[19]	ISM 915 MHz	90	24	971.5	−28.5
	ISM 2.45 GHz	210		807.3	−22.8
[20]	ISM 915 MHz	80	21	380	−26.4
	Midfield 1900 MHz	155.8		358	−23
	ISM 2.45 GHz	178.85		363	−20.47
[21]	MICS 402 MHz	80	115	936.8	−31.6
	ISM 915 MHz	60		881.2	−33.1
[26]	MICS 402 MHz	105.8	248.92	338	−46
	ISM 2.44 GHz	280.8		482	−19
[34]	MICS 402 MHz	99.98	432	129.9	−12.25
	ISM 2.45 GHz	360.15		990.7	−12.4
[35]	MICS 402 MHz	120	447	140.8	−18.5
	ISM 2.45 GHz	40		21.6	−19.5
Proposed Gosper antenna	MICS 403 MHz	126	153.67	681.0	−33.6
	ISM 915 MHz	406		383.1	−21.04
	WMTS 1400 MHz	168		603.7	−15.48
	ISM 2.45 GHz	175		568.5	−10.25

https://doi.org/10.1017/S1759078721001203 Published online by Cambridge University Press

and L_{path} (dB) is the path loss between the transmitting antenna and receiving antenna which increases with increasing the distance (d) between the transmitter and receiver at wavelength (λ).

$$L_{path} = 10\log_{10}\left(\frac{4\pi d}{\lambda}\right)^2. \quad (3)$$

If the received signal strength at the receiving antenna is greater than the receiver's sensitivity, only a reliable link can be possible. Receiver sensitivity is defined as a minimum power required by an antenna for proper demodulation of the signal. However, there is no standard definition of sensitivity level, as the receivers may have a particular sensitivity level depending on the application and requirement. Table 3 contains the link budget parameters for design consideration.

$$P_{req} = 10\log_{10}(kTB) + NF + CNR, \quad (4)$$

where kTB is defined as thermal noise power; k (Joules/K) Boltzmann's constant, T is the temperature in Kelvin, and B is the bandwidth. NF (dB) is a noise Fig. of the receiver generated by electronic circuitries and peripherals. The CNR (dB) is a channel to noise ratio similar to signal to noise ratio but calculated before the filter section of the receiver and can be expressed as

$$CNR = 10\log_{10}\left(\frac{E_b}{N_0}\right) + 10\log_{10}\left(\frac{B_r}{B}\right), \quad (5)$$

where E_b is energy per bit, N_0 (dB/Hz) is noise power density, taken from standard bit error probability curve for binary phase shift keying (BPSK) with additive white Gaussian noise (AWGN) channel, and B_r is bit rate (kbps). Finally, the link margin has been obtained by taking the difference between the receiver's available power and the minimum power required. The zone above zero is considered to be acceptable for reliable link establishment. However, some miscellaneous losses, such as mismatch loss, antenna misalignment, human error, cable loss, etc., may lead to mitigate the received signal, so for the faithful link, it is advised to consider link margin above 10 dB point.

Conclusion

A miniature size multiband antenna for implantable biomedical devices is proposed. Miniaturization is achieved by Gosper curve fractal geometry along with the shorting pin. Additionally, the Gosper curve also supports to achieve multiband resonance with the help of defected ground structure. The auxiliary arm attached to the Gosper curve helps to gain an additional frequency band. Further, a sequential nonlinear optimization technique is used to finalize the antenna design model with frequency-dependent human tissue models (skin, fat, muscle, and bone). The optimized design is investigated compared to the reference tissue model with the proposed tissue model, which shows a good agreement in the measured results. The proposed antenna has four dedicated medical bands centered at 403, 915, 1400, and 2450 MHz with quite good bandwidth values of 126, 406, 168, and 175 MHz, respectively. After that, link budget analysis has been carried out with off body antenna system. The result ensures that a good communication link can be established at a lower 1 kbps data rate as compared to 1 Mbps speed with 15 and 2 m distance, respectively, by taking 10 dB of additional margin. The maximum gain of the final design at 403, 915, 1400, and 2450 MHz are −33.6, −21.04, −15.48, and −10.25 dBi, respectively. Finally, the proposed antenna is compared with the previously reported design. The proposed Gosper antenna is novel, multiband, compact, and preserves SAR value's safety limit with input power upto 25 μW for implantable application.

Acknowledgements. This work was supported by the R & D Infrastructure Division, Department of Science and Technology, Government of India vide Order No. FST/ET-1/2018/157 (C) dated 14/03/2019.

References

1. **Jain L, Singh R, Rawat S and Ray K** (2018) Stacked arrangement of meandered patches for biomedical applications. *International Journal of System Assurance Engineering and Management* **9**, 139–146.
2. **Zhang K, Liu C, Yang X, Liu X and Guo H** (2017) An ingestible capsule system for in-body core temperature monitoring. *Microwave and Optical Technology Letters* **59**, 2670–2675.
3. **Astrin AW, Li HB and Kohno R** (2009) Standardization for body area networks. *IEICE Transactions on Communications* **E92–B**, 366–372.
4. **Federal Communications Commission:** In the Matter of Amendment of Parts 2 and 95 of the Commission's Rules in Federal Register (2009), 1–26.
5. **International Telecommunications Union-Radiocommunications (ITU-R) Radio Regulations (2016).** ITU, Geneva, Switzerland.
6. **Karacolak T, Hood AZ and Topsakal E** (2008) Design of a dual-band implantable antenna and development of skin mimicking gels for continuous glucose monitoring. *IEEE Transactions on Microwave Theory and Techniques* **56**, 1001–1008.
7. **Kim J and Rahmat-Samii Y** (2006) Planar inverted-F antennas on implantable medical devices: meandered type versus spiral type. *Microwave and Optical Technology Letters* **48**, 567–572.
8. **Soontornpipit P, Furse CM and Chung YC** (2004) Design of implantable microstrip antenna for communication with medical implants. *IEEE Transactions on Microwave Theory and Techniques* **52**, 1944–1951.
9. **Huang W and Kishk AA** (2011) Embedded spiral microstrip implantable antenna. *International Journal of Antennas and Propagation* **2011**, 1–6.
10. **Liu W-C, Chen S-H and Wu C-M** (2008) Implantable broadband circular stacked PIFA antenna for biotelemetry communication. *Journal of Electromagnetic Waves and Applications* **22**, 1791–1800.
11. **Kiourti A, Costa CA, Fernandes JR, Santiago G and Nikita KS** (2012) Miniature implantable antennas for biomedical telemetry: from simulation to realization. *IEEE Transactions on Biomedical Engineering* **59**, 3140–3147.
12. **Kumar R, Solanki LS and Singh S** (2019) Miniature Archimedean spiral PIFA antennas for biomedical implantable devices. 6th International Conference on Signal Processing and Integrated Networks (SPIN), 162–167.
13. **Hout S and Chung J-Y** (2019) Design and characterization of a miniaturized implantable antenna in a seven-layer brain phantom. *IEEE Access* **7**, 162062–162069.
14. **Yoo H and Cho Y** (2016) Miniaturised dual-band implantable antenna for wireless biotelemetry. *Electronics Letters* **52**, 1005–1007.
15. **Gani I and Yoo H** (2016) Multi-band antenna system for skin implant. *IEEE Microwave and Wireless Components Letters* **26**, 294–296.
16. **Faisal F, Zada M, Ejaz A, Amin Y, Ullah S and Yoo H** (2020) A miniaturized dual-band implantable antenna system for medical applications. *IEEE Transactions on Antennas and Propagation* **68**, 1161–1165.
17. **Luo L, Hu B, Wu J, Yan T and Xu L** (2019) Compact dual-band antenna with slotted ground for implantable applications. *Microwave and Optical Technology Letters* **61**, 1314–1319.
18. **Fan Y, Liu H, Liu X, Cao Y, Li Z and Tentzeris MM** (2020) Novel coated differentially fed dual-band fractal antenna for implantable medical devices. *IET Microwaves, Antennas & Propagation* **14**, 199–208.
19. **Shah SAA and Yoo H** (2018) Scalp-implantable antenna systems for intracranial pressure monitoring. *IEEE Transactions on Antennas and Propagation* **66**, 2170–2173.

https://doi.org/10.1017/S1759078721001203 Published online by Cambridge University Press

20. **Zada M and Yoo H** (2018) A miniaturized triple-band implantable antenna system for bio-telemetry applications. *IEEE Transactions on Antennas and Propagation* **66**, 7378–7382.
21. **Ding S, Koulouridis S and Pichon L** (2020) Design and characterization of a dual-band miniaturized circular antenna for deep in body biomedical wireless applications. *International Journal of Microwave and Wireless Technologies* **12**, 461–468.
22. **Balanis CA** (2005) *Antenna Theory – Analysis and Design*, 3rd Edn. New York: John Wiley & Sons INC.
23. **Bahl IJ and Stuchly SS** (1980) Analysis of a microstrip covered with a lossy dielectric. *IEEE Transactions on Microwave Theory and Techniques* **28**, 104–109.
24. **Ventrella J** (2012) *Root 7 Families, Brainfilling Curves-A Fractal Bestiary*. San Francisco: Eyebrain Books, 95–100.
25. **Chen CC and Wang SB** (2016) Node-Gosper curve-based unknown sensor localization using single mobile anchor in wireless sensor networks. *International Journal of Distributed Sensor Networks* **12**, 5780101.
26. **Usluer M, Cetindere B and Basaran SC** (2020) Compact implantable antenna design for MICS and ISM band biotelemetry applications. *Microwave and Optical Technology Letters* **62**, 1581–1587.
27. **Gabriel S, Lau RW and Gabriel C** (1996) The dielectric properties of biological tissues: II. Measurements in the frequency range 10 Hz to 20 GHz. *Physics in Medicine and Biology* **41**, 2251–2269.
28. **Gabriel S, Lau RW and Gabriel C** (1996) The dielectric properties of biological tissues: III. Parametric models for the dielectric spectrum of tissues. *Physics in Medicine and Biology* **41**, 2271–2293.
29. **Karacolak T, Cooper R, Unlu ES and Topsakal E** (2012) Dielectric properties of porcine skin tissue and in vivo testing of implantable antennas using pigs as model animals. *IEEE Antennas and Wireless Propagation Letters* **11**, 1686–1689.
30. **Kumar R, Solanki LS and Singh S** (2019) SAR analysis of antenna implanted inside homogeneous human tissue phantom, 6th International Conference on Signal Processing and Integrated Networks (SPIN), 755–759.
31. **IEEE** (2005) IEEE standard for safety levels with respect to human exposure to radio frequency electromagnetic fields, 3 kHz to 300 GHz, IEEE Standard C95.1.
32. **Orfanidis SJ** (2016) *Electromagnetic Waves and Antennas*. New Jersey: Rutgers University, pp. 598–633.
33. **Ma S, Bjorninen T, Sydanheimo L, Voutilainen MH and Ukkonen L** (2021) Double split rings as extremely small and tuneable antennas for brain implantable wireless medical microsystems. *IEEE Transactions on Antennas and Propagation* **69**, 760–768.
34. **Palandoken M** (2017) Compact bioimplantable MICS and ISM band antenna design for wireless biotelemetry applications. *Radioengineering* **26**, 917–923.
35. **Yeap K, Voon C, Hiraguri T and Nisar H** (2019) A compact dual-band implantable antenna for medical telemetry. *Microwave and Optical Technology Letters* **61**, 2105–2109.

Rajeev Kumar obtained his B.E degree in Electronics and Communication Engineering from the University of Rajasthan, Jaipur, India, and M.Tech in Electronics and Communication Engineering from Sant Longowal Institute of Engineering and Technology (SLIET), Longowal, Punjab, India. He has been with GIT, Jaipur, India as an Assistant Professor for 7 years. Currently he is pursuing his Ph.D degree from SLIET, Longowal, Punjab. His current research interests include antenna design and techniques, RF and microwave detection, implantable antennas for biomedical applications.

Surinder Singh (M'17) was born in Hoshiarpur, Punjab, India, in 1975. He obtained his B.Tech degree from Dr. B. R. Ambedkar Regional Engineering College, Jalandhar, in 1997, the M.Tech degree from Guru Nanak Dev Engineering College, Ludhiana, in 2003, and the Ph.D. degree from Thapar University, Patiala, India in 2007. Currently, he is working as a Professor at Sant Longowal Institute of Engineering and Technology since 2013. His field of interest is optical fiber communication and networks, antenna, and optical sensor design. He has around 145 research papers out of which 75 are in SCI international journals with Thomson Reuter impact factor and 77 are in international and national conferences. He is also handling various research projects and is a Reviewer of many international journals and conferences.

Ajay pal Singh Chauhan obtained the Engineering degree from Gulbarga University, Karnataka, India in 1994 and M.Tech degree from Punjab Technical University, Punjab, India in 2004, in Electronics and Communication Engineering. He received the Ph.D degree from Sant Longowal Institute of Engineering and Technology (SLIET), Longowal, Punjab in 2015. Dr. Singh is credited with a professional experience of more than 24 years, and currently, he is a Professor in the Department of Electronics and Communication Engineering at SLIET, Longowal, Punjab, India. He has presented and published several papers in national/international conferences and reputed journals. His research interest includes RF and microwave sensing of materials, pattern reorganization, deep learning, and computer vision.

https://doi.org/10.1017/S1759078721001203 Published online by Cambridge University Press